

Vertical Alignment of Liquid-Crystal Molecules due to Unilateral Anchoring from Charge Accumulation at the Semiconductor Interface

Hang Su,¹ Jingwen Zhang,^{1,2,*} Chao Wang,¹ Yingce Wang,¹ and Hua Zhao^{1,3,†}

¹*School of Physics, Harbin Institute of Technology, Harbin, 150001, China*

²*Key Laboratory of Micro-Optics and Photonics Technology of Heilongjiang Province, Harbin, 150001, China*

³*Key Laboratory of Micro-Nano Optoelectronic Information System, Ministry of Industry and Information Technology, Harbin 150001, China*

(Received 13 June 2019; revised manuscript received 18 October 2019; published 11 December 2019)

Recently, using good photoconductive, as-deposited ZnSe thin-film-coated ITO glass plates, excellent vertical-alignment (VA) liquid-crystal (LC) cells are prepared and excitation of visible surface plasmons is also evidenced. The interface microcosmic conditions of LCs and the alignment layer dominates macroscopical optical properties. Here, we take the mechanism as unilateral anchoring of LC molecules to the ZnSe interface mainly of (111) and using density-functional theory, the charge contributions at the interface are calculated. A strong adhesion of cyan and Zn atoms supported surface anchoring for molecules. LC cells are thus fabricated and exhibited fine original alignment with a leaked transmission as low as 0.0095% (40.2 dB) under crossed polarization. Meanwhile, the cell's bright-dark contrast ratio can reach over 1150 under a transverse electric field, along with high transparency, providing a bright prospect in readily integrating the LC layer into photonic systems, which are compatible to currently commercially successful semiconductor-based photonic and sensing applications. The cells are quite easy to fabricate and the use of a semiconductor layer makes this promising for future development.

DOI: 10.1103/PhysRevApplied.12.064029

I. INTRODUCTION

Liquid crystals (LCs) have been studied due to their incomparable electro-optic properties, especially after achieving tunable alignment in 1911 [1] and being theoretically explained in 1950 [2]. For decades, different kinds of LC molecules have been found [3] and chemically synthesized. With their unique optical properties, they are playing important roles in different fields, such as LC display [4], optical modulation [5], vortex generation [6], device controllability [7,8] by nonlinearity [9–11], large optical anisotropy and birefringence [12], and most importantly, externally electric and magnetic controlling [13–15]. As one of the key factors for judging a LC cell (LCC), the approach of alignment determines external control modes and modulation performance. It is known that LCs consist of polar molecules and thus are easily affected by interface conditions, such as substrate morphology, structure, and charged conditions. Therefore, there are a variety of routes to that end. Traditionally, LC molecules can be realized by microgrooves [16], crystalline polymer surface [17], organic mixture [18], and so forth. In fact, the introduction of foreign layers and their treatment complicate fabrication

of LC panels and cells, and this usually adversely impacts controlling the LC system. Therefore, seeking alternative approaches for easy preparation and integration is still an ever-going quest for photonics. The photoalignment method [19,20] was used widely in different applications and offered an accurate method for LC pattern and geometry controlling. The investigation into the polymer surface broadens the molecules' interaction between the alignment layer and LC layer. In recent years, graphene [21] and a graphenelike interface (*h*-BN, carbon nanotube) [22–24] supported a new method for planar alignment with π - π coupling between LC molecules and the hexagonal surface. These interface studies [21] provide smart ideas for controlling LC molecules.

To increase the response speed in an LCC, a good photoconductive semiconductor can be chosen to speed up charge-carrier transportation. As an important II-VI semiconductor material, ZnSe and ZnO has widely been investigated in preparing quantum dots [25], in making light-emitting diodes [26–28], and in exciting visible surface-plasmon polaritons (SPPs) [29]. Very recently, using electron evaporation-deposited ZnSe thin films as aligning layers without the need of any treatment, some of us have reported video-rate holography [30] and subwavelength coupling [31]. Amazed by the excellent vertical-alignment (VA) performance, achieved without

*jingwenz@hit.edu.cn

†zhaohuaz@hit.edu.cn

any foreign aligning layer and extra treatment, we took the film roughness as the underlying dictation for the VA condition in our early works. However, some further experimental results did not support this original hypothesis. For example, should the roughness dictate LC molecule alignment, the alignment would be thickness dependent, for a thicker ZnSe film shall possess a coarser surface. Contrarily, it was found that the alignments are rather always vertical no matter what the thicknesses of ZnSe films are, even down to 10 nm in thickness. Furthermore, there is no alignment of LCC made of uncoated ITO glass plates, although the ITO films possess similar roughness with thin ZnSe-coated films. Therefore, to understand why an excellent VA condition can be attained with nontreated ZnSe thin films, we have to take a closer look at the interface of the ZnSe films and LC molecules. Checking a thin ZnSe film deposited with electron-beam evaporation with a transmission electron microscope, it is found that the ZnSe film is of (111) polycrystals. In this case, the dangling bonds at the interface of the ZnSe film and the LC layer tend to attract atoms of more electronegativity, for example, N atoms in a LC molecule. In this Paper, we take into account the strong attraction of the dangling bonds to electrons of the N atoms in the cyan group of 5CB (4-cyano-4'-n-pentylbiphenyl) molecules. It is the strong attraction that forces the molecules into vertical alignment to the ZnSe (111) substrate, which supports redundant electrons in film interfaces. Based on density-functional theory (DFT), the *ab initio* calculation is used in this obvious attraction between LC molecules and ZnSe substrates. Experimentally, several LCCs are prepared and characterized optically with excellent vertical alignment. In addition, with in-plane-switching (IPS) method [32,33], quite low leaked transmission with no electric field and high transmission under an external electric voltage are achieved, leading to a large contrast ratio. Our theoretical analysis and experimental results offer an alternative LC-alignment approach and can serve as guidance in controlling LC molecules. Based on mature semiconductor-processing technology, LC layers can be readily integrated into nanophotonic systems and devices [34] since visible surface plasmons can

be supported without metallic constituents, which is highly desirable for circumventing the major hindrance associated with employment of the lossy metal part in related applications. Also, the connection between LC molecules and the semiconductor interface supports more abilities, considering that more and more SPP devices and detectors arise with graphene-LC interaction. The theoretical consideration can be easily expanded into other material systems with *ab initio* calculation. With the influence from the surrounding environment to the LC, the optical probing methodology can be used widely in grain characterizations [31] and this work broadens the structure boundaries as alignment for LCs.

II. AB INITIO CALCULATION AND ANALYSIS

To delve into the possible mechanism behind the perfect LCC VA condition achieved with an electron-evaporation deposition, we focus on the LC-ZnSe interface closely. With the development of a DFT algorithm, one can understand the electron distribution from an atomistic view and calculate the electron state after the combination of the LC molecule and ZnSe surface. In short, it is shown that the theoretical results support all the experimental results obtained to date. Our structure optimizations of the most stable geometries and charge distributions are calculated via the CASTEP computation module [35,36] based on DFT. We choose plane-wave ultra-soft pseudopotential (PWPP), generalized gradient approximation (GGA), and Perdew-Burke-Ernzerhof (PBE) approaches to take electronic effects into account. The elements are divided into two groups: (1) 5CB molecules and (2) Zn and Se atoms, shown in Fig. 1(a), in order to calculate how they are bound together. To that end, firstly, a thin slice of ZnSe (111) with three atomic layers is set as the substrate. Some proper atom numbers ($4 \times 4 \times 2$ lattices) are maintained for enough contact with the 5CB molecules. The bottom and middle atomic layers of the ZnSe substrate are fixed in position to simulate inside lattice contributions. For the substrate details, we set Zn atoms on the surface to connect with the LC molecule directly, which is a more

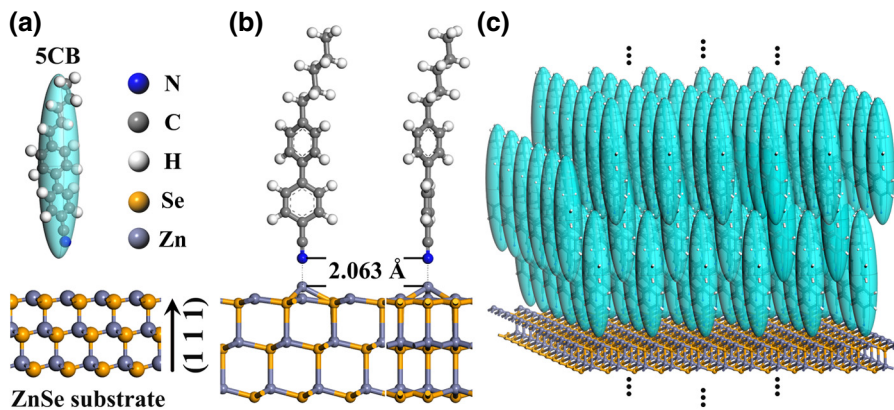


FIG. 1. (a) Schematic for LC-molecule and ZnSe-substrate structure; (b) front and side view of strong attraction between N and Zn atoms after geometric optimization and (c) vertical alignment for 5CB on ZnSe (111) films.

stable situation with only one dangling bond for the crystal boundary [37,38]. We can clearly see that this surface layer is “flatter” than the others inside in Fig. 1(b), simply because the lack of “outer” lattice attraction. The total energy of the ZnSe substrate is denoted with E_{sub} in the following calculation. Then, a 5CB molecule with a cyan as the head and a carbon chain as the tail is set above the substrate vertically with the N atom drawn nearer to the substrate surface. The total molecular energy E_m is calculated separately in advance. Furthermore, the total energy of both the molecule and the substrate E_{total} can be achieved after structural optimization [Fig. 1(b)]. Thus, the adhesion energy between the 5CB molecule and the ZnSe substrate E_b could be defined by

$$E_b = E_{\text{total}} - E_{\text{sub}} - E_m. \quad (1)$$

The distance between the N atom on the head of the 5CB molecule and the Zn atom nearby is closely monitored during geometric optimization. The distance decreases from 5 Å predefined to 2.063 Å [Fig. 1(b)] at the end of the process. During the process the nearby Zn atom shifts its position out of the original layer clearly. This displacement is a result of interaction between the 5CB molecule and the Zn atom, revealing the strong attraction force from the cyan group due to electronegativity. One sees that the stable distance is shorter than that of the typical van der Waals interaction distance of 3.4 Å, thus the adhesion energy with the value of $E_b = 1.06$ eV is much stronger than van der Waals interaction. This indicates the strong anchoring of the 5CB molecule head side to the ZnSe (111) surface. Also, we calculate the case with the single molecule lying along the surface or close to the Se atoms [39], but the results are similar: whether it is a Zn or Se atom that an N atom is near to, the head of the 5CB molecules has the tendency to displace towards its nearest Zn atom. In contrast, the substrate surface has a tendency to repel the carbon chain (tail) in a 5CB molecule. Consequently, one can simply imagine a case when a lot of molecules are approaching the substrate surface: the C≡N groups firstly combine with the nearest Zn atoms on the surface. These drawing forces are too intense to leave space for their tails to fall flat on the surface due to the small lattice distance of ZnSe (111). In fact, the distance between two Zn atoms is 4.163 Å, just a little smaller than the distance between two N atoms in LC molecules (4.677 Å). As a result, the tails of the 5CB molecules are forced to align perpendicularly to the surface [Fig. 1(c)], just like one’s hairs are electrified under a strong static electric field. After the first layer of 5CB molecules anchored strongly to the ZnSe surface, the rest of the 5CB molecules tend to align along the same direction for keeping the total inner energy the lowest, resulting in the VA condition. In other words, all the 5CB molecules are standing perpendicularly to the substrate statistically. In fact, after preparation of the ZnSe film, the dangling

bonds on the surface should be combined quickly with a layer of molecules or ions in air (for example, N₂) after exposure to ambient air. When the LC molecules connected to the surface, the cyan would compete for the dangling bonds with absorption layer. But the adsorption-desorption process is dynamic [40]. This dynamic process would be intensified under elevated temperature, which is necessary for filling LC into cells due to capillary effect. Thus, N atoms in LC molecules have more possibility to seize dangling bonds due to more energy release with the help of thermal motion and dynamic absorption process.

Bearing in mind the result of huge adhesion energy, there must be charge distribution during the adhesion process. Here we analyze the system’s charge redistribution and electron transfer with total electron density and electron density difference, shown in Figs. 2(a) and 2(b), respectively. Figure 2(a) shows the total electron density before (left part) and after the adhesion process (right part). From these results one can find that the total electron density fuses into each other’s connection part, i.e., there is a strong connection (similar to a chemical bond) between the N atom in the cyan group and its adjacent Zn atom. This reveals that after the adhesion process, the molecule and the substrate have become “one unit” owing to the

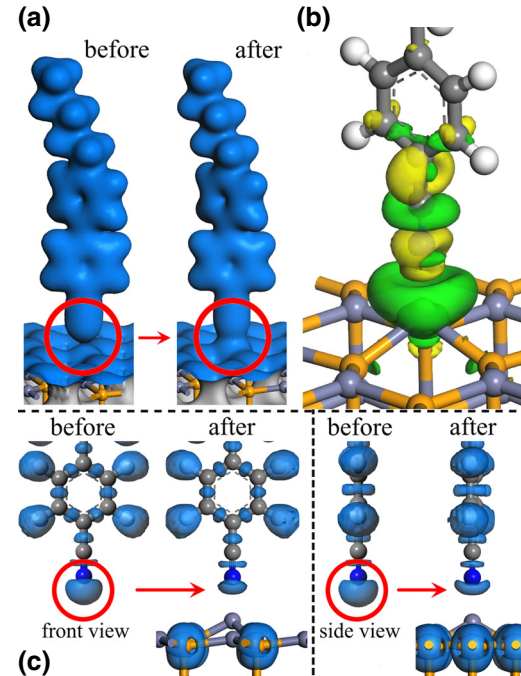


FIG. 2. Charge distribution in the interaction of the LC molecule and ZnSe substrate: (a) total electric density before and after two groups stable with geometry optimization; (b) electron-density difference and transportation during the stable process, where green means electron reduction and yellow means enhancement; (c) electron-charge localization before and after adhesion at different view, where the accumulation near N atoms has changed a lot.

electron transferring between the cyan and the substrate. Figures 2(b) and 2(c) show the electron-density difference and electron-charge localization before and after the molecule-substrate combination, from which one can get a clear picture regarding how the charges transfer in the stable condition after the adhesion process does. The two unbonded electron pairs and the C≡N triple bond are on either side of the N atom, which are shown as a hemisphere and a ring in Fig. 2(c). Compared with that after the adhesion, this “hemisphere” localization has transformed obviously under the effect of surface-dangling bonds. If we set the molecule and the substrate as two groups, the electron-density difference of the groups [Fig. 2(b)] could help us understand the adhesion process from group to group. The density near the N atom decreases and transfers to the region where the Zn atom is and forms a covalent-like bond, which pulls the molecule and Zn atom closer to a distance that even shorter than Zn—Se bond length. At the same time, the substrate surface is full of “dangling” bonds, anchoring the molecule heads down and forcing LC molecules’ tails up away from the surface. This kind of charge transferring also occurs in a similar situation between LC molecules and graphene or graphenelike structures [24], meaning two π - π stackings with approximately 2 eV energy release but middle attraction in an entire molecule. In our structure, the attraction is unilateral, and the substrates are lacking π bonds on the surface, which is leading to a perpendicular orientation.

III. EXPERIMENTAL RESULTS AND DISCUSSION

Owing to unilateral anchoring of the cyan group to the ZnSe film surface, the primary layer of 5CB molecules are forced to stand perpendicular to the ZnSe films and results in a VA condition in macroscopic view. Therefore, one can examine the VA performance by using optical

measurements that follow. The ZnSe films coated on ITO glasses are checked by XRD methodology and the experimental results are shown in Fig. 3(a). One notes that if the ITO glass spectrum (blue line) is removed from that coated with ZnSe, most ZnSe grains are of (111) orientation and little of (311). A designed LCC [Fig. 3(b)] with partially etched off ITO-ZnSe glasses is prepared to examine how good a VA condition is. The remaining ITO films covered two opposite edges on the surface in order to apply an in-plane transverse electric field in the following experiments. The preparation methods are stated in the [Appendix](#) for details. During the preparing process, LC filled the cell from one edge to the end and a clear liquid-air interface can be observed. It is very interesting that LC moved faster and looked less opaque in the region with coated ZnSe films than that with ITO film alone [39]. This phenomenon confirms the strong attraction of the ZnSe films to the 5CB molecules, without excluding the wetting effect of the 5CB to the ZnSe. The fineness of alignment can be checked simply with a polarization microscope and a typical picture is shown in Figs. 3(c)–3(g) with different angles between polarizer and analyzer. It is interesting to notice that there are three regions in the photograph presenting different alignment boundary conditions from left to right in the cross-polarization case [Fig. 3(c)]: (1) with two layers of ITO films; (2) with one layer of ZnSe film and one ITO; and (3) with two ZnSe layers. The LC-molecule orientations are totally chaotic with “ITO alignment film” whatever the P-A angles are, thus this region shows a typical nonalignment characteristic. With only single anchoring layer ZnSe film, the middle region (dark field) offers a rather good alignment compared to the left region yet not as excellent as that with double anchoring layers shown in the right region (darker field). With the P-A angle changing from 90° to 0° [Figs. 3(d)–3(g)], the illuminated area becomes bright at the ZnSe region and there are almost

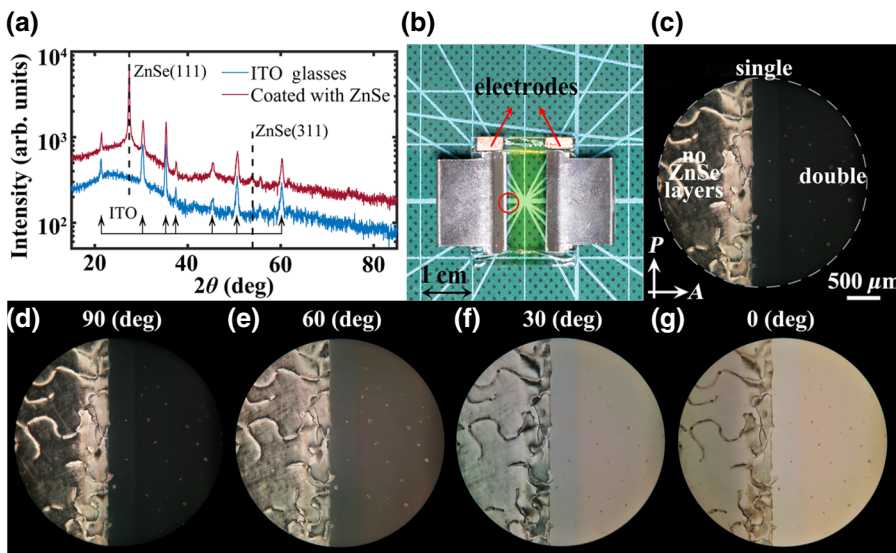


FIG. 3. (a) XRD patterns of the ITO-ZnSe film substrate, which is used to prepare the LC cell in the following experiments; (b) a picture of an LCC; (c) microscopic picture of an edge circled in (b), where three regions correspond to “no ZnSe film,” “single film,” and “double films” as the alignment layer from left to right, respectively; (d–g) pictures of the same position with the angles between polarizer (P) and analyzer (A) of (d) 90°, (e) 60°, (f) 30°, and (g) 0°.

no changes in the left region. In this condition, the difference between the single and double layer becomes obvious due to the absorption of ZnSe. These pictures demonstrate isotropy with ZnSe-aligning layers.

Here we use a simple cross-polarization optical system in characterizing the alignment of the LCC, shown in Fig. 4(a). The LCC is illuminated with an expanded laser beam (561 nm) and an analyzer perpendicular to the incident beam is placed after the LCC. The polarization of incident laser is along the x -axis direction and the transmission is defined as 100%. The polarizer is placed normally to prevent other modes coming from the laser cavity. The beam-propagating direction is defined as the z axis and the beam's electric field vibrates along the x axis due to the orthogonal polarizer. Upon turning the analyzer parallel to the y axis, a power meter (Thorlabs, PM110D) is monitoring the transmission light to represent the effects of the LCC on the incident light beam. Originally, the LC layer is treated as a uniaxial crystal with refractive index $[n_o, n_o, n_e]$ ($n_o = 1.51$ and $n_e = 1.71$ from Ref. [41]), whose optical axis is coaxial with the LCC surface normal. Thus, the LC layer does not affect the incident light polarization as long as it propagates along the z axis, and hence an extremely low leaked transmission is received after the analyzer. The

results are shown in Fig. 4(b) (circle B). The transmissivities are all as equally low as around 0.0095% (40.2 dB). Actually, they are even lower than that without the samples (circle A). This resulted from the absorption of ZnSe layers at 561 nm. When the LCC is placed off axis whose surface normal has an angle of 18.9° with incident beam, an anisotropy is induced from the LC layer optical axis to the x - y plane. As a result, a curve from 0.01 to 0.6% can be monitored versus rotation angle. We can obtain clear peaks at $45^\circ, 135^\circ, 225^\circ$, and 315° and valleys at $0^\circ, 90^\circ, 180^\circ$, and 270° , demonstrating excellent crystal orientation in the samples. Both the transmission curves of circles A and B indicate the perfect vertical alignment in the LC layer.

Based on good VA and a crossed polarization system, a simple phase-shift-transmission modulator can be implemented using LC-molecule polarity. It is well known that the LC layer's optical axis can be twisted with an external electric field, which serves as the backbone in display and optical modulators and filters. In the so-called IPS method, a transverse electric field is applied in the x - y plane and the orientation of LC molecules is twisted along the field direction depending on the magnitude of external electric field. For an extreme case that the layer's LC director (optical axis) is turned totally in the x - y plane, the permittivity

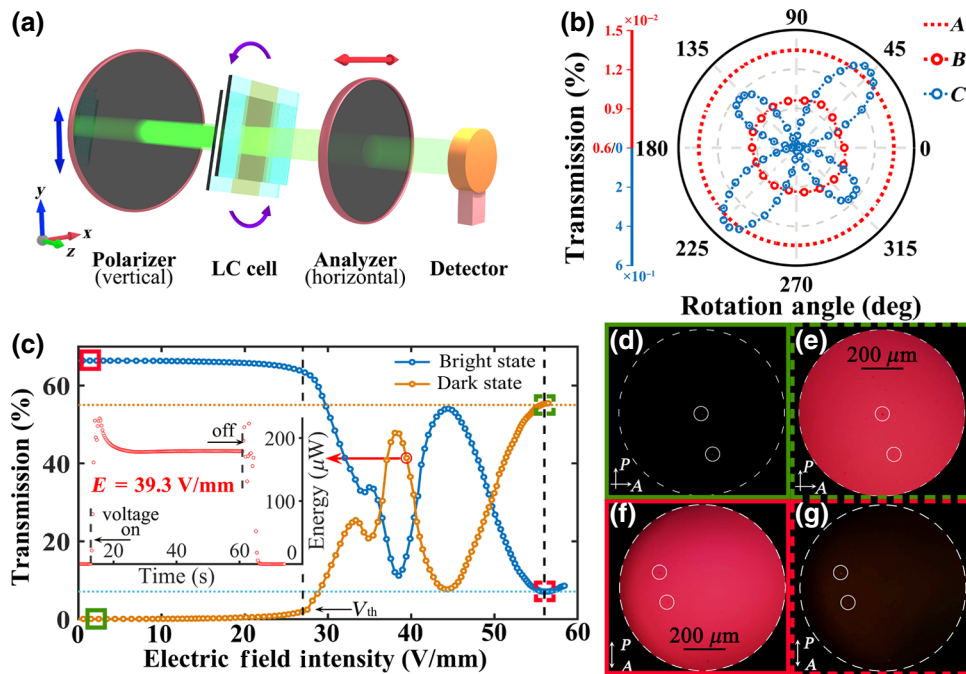


FIG. 4. (a) Experiment arrangements of crossed-polarized system; (b) transmission of the LC cell with different rotation angles θ at normal (line B) or oblique incidence (line C) conditions. Line A is the transmission without the LC cell. Two color lines have different scales and are shown on left; (c) transmission with different external electric field, where $\theta=45^\circ$. The inset in (c) is transmission energy-time graph at the condition of 39.3 V/mm electric field, corresponding to the red marked circle in (c); (d–g) polarized optical microscopy (POM) at the center of sample in the dark state (P and A are perpendicular) without (d) and with (e) voltage applied and in the bright state (P and A are parallel) without (f) and with (g) voltage applied, corresponding to squared positions with green solid (d), green dashed (e), red solid (f), and red dashed (g) lines marked in (c), respectively. The white circles in (d–g) are defects on the glass plates.

tensor to describe the LC layer is transformed from

$$\varepsilon_{\text{off}} = \begin{bmatrix} 2.25 & 0 & 0 \\ 0 & 2.25 & 0 \\ 0 & 0 & 2.89 \end{bmatrix}, \quad (2)$$

to

$$\begin{aligned} \varepsilon_{\text{on}} = \varepsilon' &= (\mathbf{A})(\varepsilon_{\text{off}})(\mathbf{A})^{-1} = \begin{bmatrix} \cos \theta & \sin \theta & 0 \\ -\sin \theta & \cos \theta & 0 \\ 0 & 0 & 1 \end{bmatrix} \\ &\times \begin{bmatrix} 2.25 & 0 & 0 \\ 0 & 2.25 & 0 \\ 0 & 0 & 2.89 \end{bmatrix} \begin{bmatrix} \cos \theta & -\sin \theta & 0 \\ \sin \theta & \cos \theta & 0 \\ 0 & 0 & 1 \end{bmatrix}, \end{aligned} \quad (3)$$

where θ is the angle between the optical axis and the x axis. Here we simplify the transition to a limiting case that all the molecules are twisted from the original VA to a planar alignment. In our experiment, we set $\theta=45^\circ$ to affect the most on the incident polarization. As a result, the director of the LC layer rotates from originally along the z axis to 45° in the x - y plane gradually with increasing external electric field. In this illumination condition, if we treat the LC layer as a simple birefringence crystal, the transmissivity after passing a crossed polarizer can be expressed as

$$T_{\perp} = \frac{1}{2} \left[1 - \cos \left(\frac{2\pi d \cdot \Delta n}{\lambda} \right) \right], \quad (4)$$

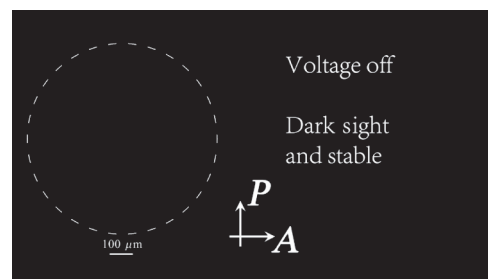
where Δn is the refractive index difference at the x and y axes, d is the thickness of LC layer, and λ is incident light wavelength. Δn increases to 0.2 maximum with increasing the external voltage. The thickness of the samples we use in the experiment is $31 \mu\text{m}$, resulting in multiple maximums and minimums with increasing the external voltage for incident beams at 561 nm . The transmissivity is nearly zero with no voltage applied and increases significantly with a certain voltage, leading to a dark-to-bright state transition. Similarly, if we place the analyzer parallel to the polarizer, there is a decreasing for the transmissivity and it can be expressed theoretically as

$$T_{\parallel} = \frac{1}{2} \left[1 + \cos \left(\frac{2\pi d \cdot \Delta n}{\lambda} \right) \right]. \quad (5)$$

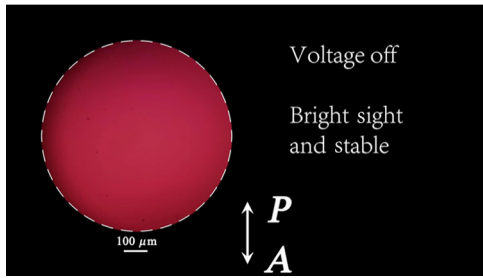
The relationship of the transmissivity versus external field measured in experiment is shown in Fig. 4(c). It is seen that a phase difference is introduced into the incident beam due to director turning and the beam polarization is twisted with an angle ψ when passing through the cell. The polarization twisting generates a component in the analyzer direction, resulting in a rising transmissivity shown

in Fig. 4(c). One notes the transmissivity increased dramatically when the voltage was over the threshold, which was 28 V/mm , and the transmissivity reaches its maximum at 43 V/mm with 56%. Encouragingly, our LCC modulation contrast ratio between the bright and dark field $r = (I_{\text{bright}}/I_{\text{dark}})$ is 1150 under this condition, which is quite large for a modulator. It should be noted that I_{dark} used here is that during modulation, which is about 0.05% due to analyzer angle error and also, the beam normally incident on the sample, meaning that the transmission is not minimum due to the tilt angle. If the minimum of leaked transmission (0.0095%) is used for modulation depth, the contrast ratio can achieve nearly 6000, which means there is still wide room for improvement. There is a small loss of energy after passing through the polarizer, which is due to the fact that the laser consists of other polarizations and the reflection of the polarizer and analyzer. We find that the maximum transmission is 82.8% with parallel polarization without the LC cell and 66.9% with the cell, which limits the modulation depth of our LC cells. The transmission can be enhanced with antireflection films. Thus, our system can be readily integrated into many photonic systems and devices simply due to the maturity in deposition of the semiconductor layer. Also, we take pictures of the microscope at the center of LC cells, as shown in Figs. 4(d)–4(g). From Eqs. (4) and (5) one can tell the LC layer electric response is related with incident wavelength, meaning our cells are tunable for full band. Thus, a 632-nm source is applied in polarized optical microscopy (POM). Figures 4(d) and 4(e) show optical behaviors with crossed polarization (dark state) under the conditions of no voltage (d) and a certain voltage applied (e). For parallel polarization (bright state), (f) and (g) show POM without and with voltage applied, respectively. The POM brightness fits to the experiment results very well and reveals large areas uniformity under an external field. Also, the electric response process (dark state and bright state) of the LC cell with voltage applying is supported in Videos 1 and 2. The videos are played in slow motion with a scale of 0.5 for better observation.

As we briefly stated in the introduction section, the SPP excitation was evidenced in the ZnSe-LC system.



VIDEO 1. LCC electric response in dark state (P and A are perpendicular).



VIDEO 2. LCC electric response in bright state (P and A are parallel).

After discussion regarding the highly possible mechanism behind this easier and perfect VA, it is beneficial to cover the charge accumulation at the ZnSe-LC interface. As aforementioned, a thin ZnSe film consists of tiny ZnSe (111) grains. The LC molecules align perpendicular to the ZnSe surface, resulting from a strong combination of the N and Zn atoms, stemming from surface-dangling bonds and electronegativity. The distance between two Zn atoms on the surface is slightly smaller than the average spacing of 5CB molecules at 25 °C. The molecules have to stand on the surface because the N sides can be anchored near the Zn atoms while rejecting the others. It should be noted that these LC molecules are only connected to the atoms on the surfaces, which means that the alignment layer (ZnSe film) can be made extremely thin, even to a few nanometers. In our experiment the alignment layers are controlled as approximately 30 nm to guarantee a uniform film coated on the ITO glass. At the same time, one dangling bond contains an extra electron, which is also anchored by the nearby LC molecule. These electrons on the surface form 2DEG with a density of around $N = 1.07 \text{ C/m}^2$, which is high enough to support UV to visible SPP at the interface of LC-ZnSe [29,31]. The anions originating from LC and electrons from ZnSe film indeed reduce the electrons' adhesion greatly, therefore, one can expect that a quite free electrons swarm at the interface, which can be regarded as 2DEG. In other words, near the LC-ZnSe interface, a metalliclike nanometer layer is formed. The surface electron density might decrease due to absorption of the remaining micro molecules, but this electron layer's effect cannot be ignored. This mechanism provides a promising coupling method on plasmonic devices with LC modulation and to observe SPPs on a semiconductor-LC interface [30,31]. The resultant electromagnetic field enhancement can influence adjacent LC molecules. The permittivity and dispersion can be estimated using the Drude model with charge density mentioned above [42]:

$$\begin{aligned} \epsilon_m &= \epsilon_\infty - \frac{\omega_p^2}{\omega^2 + i\gamma\omega} = \epsilon_\infty - \frac{e^2 N}{\epsilon_0 m_{\text{eff}}(\omega^2 + i\gamma\omega)} \\ &= \epsilon_r + i\epsilon_i \end{aligned} \quad (6)$$

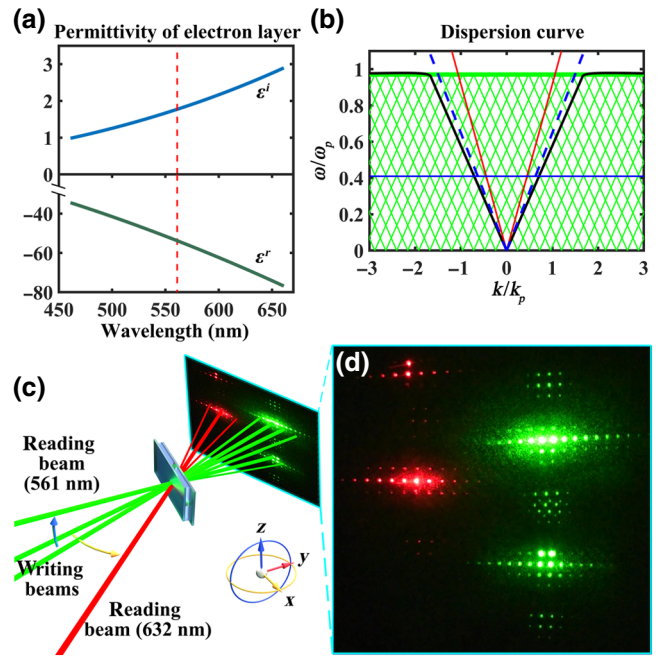


FIG. 5. Calculated value of electron layer's permittivity (a), wave-vector matching (b), and multiple diffraction patterns based on ZnSe VA LCC in 2BC experiment. The red dashed line in (a) and blue solid line in (b) correspond to 561 nm incident beam. (c), experimental arrangements for SPP coupling. In diffraction patterns (d), we use a red beam (632 nm) as the reading beam and the multiple diffractions in both transmission patterns (left center) and reflection patterns (left top) indicate light-SPP coupling at the interface ZnSe-LC.

and the electron accumulation layer performs a metallike optical properties, shown in Fig. 5(a), which means that the light can be coupled into surface waves just in this layer under proper conditions, for example, phase gratings formed in LC layer using two-beam-coupling (2BC) experiment. Figure 5(b) shows the band structure of the 2DEG-supported SPPs. The crossed points of laser light (blue solid horizontal line) and dispersion curve hint bidirectional coupling around those points and diffraction patterns between the parallel component of incident light k_x and SPPs, which can be expressed as [43] $k_{\text{SPP}} = k_x + \Delta k = k_x + m(2\pi/\Lambda)$, $m = \pm 1, \pm 2, \pm 3, \dots$ corresponding to the different diffraction orders shown in Fig. 5(d). Here Λ is the grating spacing. We use two crossover 561 beams' interference [0.4°, writing beams in Fig. 5(c)] and formed a phase grating in the LC layer. Regarding the phase-grating mediated SPPs' excitation, one knows that once a phase grating is written with two coherent laser beams at 561 nm, it can excite SPPs at the same frequency. The SPPs can be coupled back into propagating light, and hence results in a 2D diffraction pattern in the same frequency. Once a third laser beam at 561 nm, which is also coherent to the two writing laser beams mentioned above, the diffraction pattern is

expanded vertically with more orders [Figs. 5(c) reading beam (561 nm) and 5(d) small green patterns]. When another reading beam at 632 nm (Fig. 5(c) reading beam 632 nm) illuminated the phase-grating area, SPPs at the same frequency are excited and coupled back to propagating beams, resulting in a 2D red diffraction pattern on the left side shown in Fig. 5(d) red parts. With applying external electric field (approximately 10 V) on the two surfaces of the LC cell, we observe multiple orders with the incident beams for the center, the green part shown in Fig. 5(d). Similarly, the diffraction orders are also observed with a red signal light at 632 nm [Fig. 5(d) red part]. The reflection and transmission patterns (for the green part, top part is transmission and bottom part is reflection; contrary positions for red part) demonstrate the bidirectional coupling between SPP and lights.

The anchoring energy and tilt angle are two important parameters for a LC cell, so we measure them and present here. Firstly, for a VA LC cell the tilt angle could be obtained with the minimum transmission in a crossed-polarization system [44] when the incident angle is changing. The result is $1.38(1)^\circ$ to sample normal, meaning the tilt angle in our cells is $90 - 0.89(5) = 89.10(5)^\circ$ with Snell's law applying [39]. According to the effective cell-gap method [45–47], the anchoring energy can be estimated by the threshold voltage V_{th} and the electricity responding times τ_r and τ_f . Thus, several samples are prepared and their anchoring energies are measured, fell in a small range, with a result of $1.1(5) \times 10^{-5} \text{ J/m}^2$ in average. Considering the photoconductivity of ZnSe and the electron pair near N atoms, the electron density on the surface may be higher than that only calculated by dangling bonds, which also induces much more complicated phenomena. Our LCCs exhibit intense modulation function and the maximum transmission, which is almost double traditional VA LCC (about 30% transmission [21]). This means that our cells can be used in display systems with high transparency and large modulation depth. Also, the antireflection films can increase the transmission, which is a mature technology nowadays.

IV. CONCLUSION

In conclusion, we elucidate the highly possible origin behind the excellent VA for LCCs, made of an electron evaporation-deposited ZnSe-coated substrate. Without any treatment, the as-deposited ZnSe films are of (111) grains. With *ab initio* calculation, a strong attraction between the N atoms in 5CB molecules and the Zn atoms at the interface is revealed. The electron transition between atoms explains the huge adhesion energy (1.06 eV) for a single molecule pair. The unilateral attraction from the substrate results in VA for the LC layer. Using an LCC prepared with these substrates, we demonstrate remarkably high-quality alignment and electro-optic modulation with an

unambiguous threshold voltage and with an extremely large contrast ratio (approximately 1150) at a proper external electric field. Meanwhile, the transmission of the LCC under zero applied field is almost completely dark (0.0095%), whereas as high as 56% transmission is achieved upon applying a suitable electric voltage, showing great improvement for some devices [21,48], whatever the initial alignments of the LCCs are. The ZnSe-LC system can be readily integrated into other photoelectric devices naturally. Moreover, the ZnSe-LC system can support visible SPPs, which is promising for broad applications with nanometric waveguides, modulators, sensors and detectors [49], and photonic circuits [6]. One can simply design and fabricate a metasurface [34] on the ZnSe layer and control the optical and electrical responses with the LC layer. This is readily applicable in designing tunable metasurfaces.

ACKNOWLEDGMENTS

This work is partly supported by the grant of National Natural Science Foundation of China under Project Nos. 61875050 and 11374076.

H.Z. and H.S. initiated the idea. H.S. finished the model for DFT software calculation and results' analysis. H.S. and C.W. performed the experiments. H.S. and Y.W. analyzed and interpreted data. H.S and J.Z. wrote the manuscript. H.Z. supervised the project.

APPENDIX

ITO glass pretreatment: the glasses ($20 \times 20 \text{ mm}^2$, South China Xiang Science & Technology Company) are coated with 185-nm ITO films using CVD technology. The glasses are photoetched (ultraviolet photoetching machine, model URE-2000/35, Institute of Optoelectronic Technology, Chinese Academy of Sciences) with acid to obtain a gap of 8 mm between the two electrodes on the same plane to prevent short circuit. Then the ZnSe film is coated on ITO glasses with electron-beam evaporation at 70 degree centigrade with a thickness of 30 nm at the position that ITO are etched off (Model LJ-550E, from LJ-UHV Technology, Inc.) Under a condition of accelerating voltage at 8.0 kV and substrate-holder rotary speed at 20 rpm, and deposition rate at 3.0 Å/s. Coated ZnSe film is characterized as 34 nm with a stylus profilometer (Model XP-100, Ambios Technology, Inc.). As a result, the glasses are separated to three strips: the two electrodes at two edges and an ZnSe film of 8 mm in length in the middle.

ZnSe lattice orientation test: the crystal orientation of ZnSe films coated onto ITO glasses is determined by x-ray diffraction analysis (model XD-D1, Shimadzu).

Liquid crystal cell (LCC) preparation: two pieces of glass plates are covered together with ZnSe films face to face. The four electrodes are parallel to each other and we

use two spacers with 31 μm thickness placed at the electrodes side to control the cell's interspace. Also, the two ITO glasses are displaced around 2 mm in the electrode direction. After fixing the two glass plates, the empty cell is ready to fill liquid crystal (5CB, Merck Co.) at 100 degree centigrade from the one edge, which needs to be sealed with sealant (PDMS, SYLGARD 184 silicone elastomer, Dow Corning Co.) at 110 degree centigrade and 20 min after filling. Then the LCC is kept for 1 h at elevated temperature and then was cooled and reheated up several times to eliminate effects from impurities on ZnSe surfaces in an airtight box.

Detector and photo devices: the intensities of laser beams are monitored with a power meter (PM110D, Thorlabs Co.) and all photographs above are captured by Nikon D750, NIKKOR AF 50 mm f/1.8D camera lens and macro adapter ring (BR-2A, Nikon Co.).

Transmission varies with incident angles: the incident light is settled still and we rotate the sample from -20° to 20° , where 0° means the sample normal and the incident light are coaxial. The transmission is monitored by a power meter (PM110D, Thorlabs Co.) and the sample is placed and fixed on a rotation plate (Continuous 360° Motorized Rotation, HDR50, Thorlabs Co.).

- [1] C. Mauguin, Sur les cristaux liquides de Lehmann, *Bul. Soc. Fr. Miner.* **34**, 71 (1911).
- [2] V. H. De, Rotatory power and other optical properties of certain liquid crystals, *Acta Crystallogr.* **4**, 219 (1951).
- [3] G. Friedel, Les états mésomorphes de la matière, *Ann. Phys.* **9**, 273 (1922).
- [4] T. J. Scheffer and J. Nehring, A new, highly multiplexable liquid crystal display, *Appl. Phys. Lett.* **45**, 1021 (1984).
- [5] S. S. Li, Z. J. Wu, and F. Xu, Measurement of surface plasmon polariton enhanced goos–hanchen shift based on grating and liquid crystal technologies, *IEEE Photonic Tech. L* **23**, 1829 (2011).
- [6] N. Kravets, N. Podoliak, and M. Kaczmarek, Self-induced liquid crystal q-plate by photoelectric interface activation, *Appl. Phys. Lett.* **114**, 061101 (2019).
- [7] P. J. Collings and J. S. Patel, *Handbook of Liquid Crystal Research* (Oxford University Press, New York, 1997).
- [8] J. Stöhr, M. G. Samant, and J. Lüning, Liquid crystal alignment on carbonaceous surfaces with orientational order, *Science* **292**, 2299 (2001).
- [9] A. Minovich, J. Farnell, D. N. Neshev, et al., Liquid crystal based nonlinear fishnet metamaterials, *Appl. Phys. Lett.* **100**, 121113 (2012).
- [10] X. Zhuang, P. B. Miranda, and D. Kim, Mapping molecular orientation and conformation at interfaces by surface nonlinear optics, *Phys. Rev. B* **59**, 12632 (1999).
- [11] I. C. Khoo, C. W. Chen, K. L. Hong, et al., Nonlinear optics of nematic and blue phase liquid crystals, *Mol. Cryst. Liq. Cryst. Sci. Technol.* **594**, 31 (2014).
- [12] C. Williams, Y. Montelongo, and J. O. Tenorio-Pearl, Engineered pixels using active plasmonic holograms with liquid crystals, *Phys. Status. Solidi-R.* **9**, 125 (2015).
- [13] J. Sautter, I. Staude, and M. Decker, Active tuning of all-dielectric metasurfaces, *ACS Nano* **9**, 4308 (2015).
- [14] L. Lucchetti, K. Kushnir, and V. Reshetnyak, Light-induced electric field generated by photovoltaic substrates investigated through liquid crystal reorientation, *Opt. Mater.* **73**, 64 (2017).
- [15] D. K. Yang, *Fundamentals of Liquid Crystal Devices* (John Wiley & Sons, Chichester, West Sussex, UK, 2014).
- [16] D. W. Berreman, Solid Surface Shape and the Alignment of an Adjacent Nematic Liquid Crystal, *Phys. Rev. Lett.* **28**, 1683 (1972).
- [17] J. M. Geary, J. W. Goodby, and A. R. Kmetz, The mechanism of polymer alignment of liquid-crystal materials, *J. Appl. Phys.* **62**, 4100 (1987).
- [18] M. F. Toney, T. P. Russell, and J. A. Logan, Near-surface alignment of polymers in rubbed films, *Nature* **374**, 709 (1995).
- [19] J. Y. Ho, V. G. Chigrinov, and H. S. Kwok, Variable liquid crystal pretilt angles generated by photoalignment of a mixed polyimide alignment layer, *Appl. Phys. Lett.* **90**, 243506 (2007).
- [20] V. G. Chigrinov, V. M. Kozenkov, and H. S. Kwok, *Photoalignment of Liquid Crystalline Materials: Physics and Applications* (John Wiley & Sons, Chichester, West Sussex, UK, 2008).
- [21] K. H. Kim, B. W. Park, and S. W. Choi, Vertical alignment of liquid crystals without alignment layers, *Liq. Cryst.* **40**, 391 (2013).
- [22] P. Blake, P. D. Brimicombe, and R. R. Nair, Graphene-based liquid crystal device, *Nano Lett.* **8**, 1704 (2008).
- [23] R. Basu and L. J. Atwood, Two-dimensional hexagonal boron nitride nanosheet as the planar-alignment agent in a liquid crystal-based electro-optic device, *Opt. Express* **27**, 282 (2019).
- [24] K. A. Park, S. M. Lee, and S. H. Lee, Anchoring a liquid crystal molecule on a single-walled carbon nanotube, *J. Phys. Chem. C* **111**, 1620 (2007).
- [25] M. Danek, K. F. Jensen, and C. B. Murray, Synthesis of luminescent thin-film CdSe/ZnSe quantum dot composites using CdSe quantum dots passivated with an overlayer of ZnSe, *Chem. Mater.* **8**, 173 (1996).
- [26] H. Okuyama, T. Miyajima, and Y. Morinaga, ZnSe/ZnMg SSe blue laser diode, *Electron. Lett.* **28**, 1798 (1992).
- [27] B. Zhao, Y. Yao, and M. Gao, Doped quantum dot@ silica nanocomposites for white light-emitting diodes, *Nanoscale* **7**, 17231 (2015).
- [28] Y. Fan, J. Han, and L. He, Graded band gap ohmic contact to p-ZnSe, *Appl. Phys. Lett.* **61**, 3160 (1992).
- [29] T. Xue, H. Zhao, and C. Meng, Impact of surface plasmon polaritons on photorefractive effect in dye doped liquid crystal cells with ZnSe interlayers, *Opt. Express* **22**, 20964 (2014).
- [30] H. Zhao, C. Lian, and F. Huang, Impact of grating spacing and electric field on real time updatable holographic recording in nanoscale ZnSe film assisted liquid crystal cells, *Appl. Phys. Lett.* **101**, 211118 (2012).

- [31] H. Zhao, T. Xue, and H. Su, Subwavelength coupling strengthened optical amplification in nematic liquid crystal cells, *Appl. Phys. Lett.* **111**, 111602 (2017).
- [32] R. A. Soref, Field effects in nematic liquid crystals obtained with interdigital electrodes, *J. Appl. Phys.* **45**, 5466 (1974).
- [33] S. H. Lee, S. L. Lee, and H. Y. Kim, Electro-optic characteristics and switching principle of a nematic liquid crystal cell controlled by fringe-field switching, *Appl. Phys. Lett.* **73**, 2881 (1998).
- [34] H. Su, H. Wang, and H. Zhao, Liquid-crystal-based electrically tuned electromagnetically induced transparency metasurface switch, *Sci. Rep.* **7**, 17378 (2017).
- [35] M. D. Segall, P. J. Lindan, and M. A. Probert, First-principles simulation: Ideas, illustrations and the CASTEP code, *J. Phys.: Condens. Mat.* **14**, 2717 (2002).
- [36] S. J. Clark, M. D. Segall, and C. J. Pickard, First principles methods using CASTEP, *Z. Krist. -Cryst. Mater.* **220**, 567 (2005).
- [37] M. Shiojiri, C. Kaito, and S. Sekimoto, Polarity and inversion twins in ZnSe crystals observed by high-resolution electron microscopy, *Philos. Mag. A* **46**, 495 (1982).
- [38] N. Matsumura, K. Maemura, and T. Mori, Molecular beam epitaxial growth of ZnSe (111) films on misoriented GaAs (111) A substrates, *J. Cryst. Growth* **159**, 85 (1996).
- [39] See the Supplemental Materials at <http://link.aps.org/supplemental/10.1103/PhysRevApplied.12.064029> for interactions of different relative space positions, dynamic process of filling and tilt angle presentation.
- [40] I. Langmuir, The constitution and fundamental properties of solids and liquids. Part I. Solids., *J. Am. Chem. Soc.* **38**, 2221 (1916).
- [41] V. Tkachenko, G. Abbate, and A. Marino, Nematic liquid crystal optical dispersion in the visible-near infrared range, *Mol. Cryst. Liq. Cryst. Sci. Technol.* **454**, 263 (2006).
- [42] H. Zhao, Y. Wang, and T. Xue, Direct evidence of visible surface plasmon excitation in ITO film coated on LiNbO₃ slabs, *Opt. Express* **25**, 6227 (2017).
- [43] S. Hayashi and T. Okamoto, Plasmonics: Visit the past to know the future, *J. Phys. D: Appl. Phys.* **45**, 433001 (2012).
- [44] G. Baur, V. Wittwer, and D. W. Berreman, Determination of the tilt angles at surfaces of substrates in liquid crystal cells, *Phys. Lett. A* **56**, 142 (1976).
- [45] L. M. Blinov and V. G. Chigrinov, *Electrooptic Effects in Liquid Crystal Materials* (Springer Science & Business Media, New York, 1996).
- [46] X. Nie, R. Lu, and H. Xianyu, Anchoring energy and cell gap effects on liquid crystal response time, *J. Appl. Phys.* **101**, 103110 (2007).
- [47] E. Jakeman and E. P. Raynes, Electro-optic response times in liquid crystals, *Phys. Lett. A* **39**, 69 (1972).
- [48] G. J. Choi, D. G. Ryu, and J. S. Gwag, Anchoring strength of indium tin oxide electrode used as liquid crystal alignment layer, *J. Appl. Phys.* **125**, 064501 (2019).
- [49] M. A. Shehzad, S. Hussain, and J. Lee, Study of grains and boundaries of molybdenum diselenide and tungsten diselenide using liquid crystal, *Nano Lett.* **17**, 1474 (2017).